LAWRENCE
LIVERMORE
NATIONAL
LABORATORY

LLNL-JRNL-746745

KOHN ANOMALY AND PHASE STABILITY IN GROUP-VB TRANSITION METALS

A. Landa, P. Soderlind, I. I. Naumov, J. E. Klepeis, L. Vitos

February 23, 2018

Computation

Disclaimer

computation

MDPI

Review

Kohn Anomaly and Phase Stability in Group VB Transition Metals

Alexander Landa [1,*], Per Söderlind [1], Ivan I. Naumov [2], John E. Klepeis [1] and Levente Vitos [3,4,5]

[1] Physics Division, Lawrence Livermore National Laboratory, Livermore, CA 94551, USA; soderlind1@llnl.gov (P.S.); klepeis1@llnl.gov (J.E.K.)
[2] Geophysical Laboratory, Carnegie Institution of Washington, Washington, DC 20015, USA; inaumov@carnegiescience.edu
[3] Department of Materials Science and Engineering, Royal Institute of Technology, SE-100 44 Stockholm, Sweden; levente@kth.se
[4] Wigner Research Center for Physics, Institute for Solid State Physics and Optics, PO Box 49, H-1525 Budapest, Hungary
[5] Department of Physics and Astrinomy, Uppsala University, Box 516, SE-75120 Uppsala, Sweden
* Correspondence: landa1@llnl.gov; Tel.: +1-925-424-3523

Received: 28 February 2018; Accepted: 21 March 2018; Published: 26 March 2018

Abstract: In the periodic table, only a few pure metals exhibit lattice or magnetic instabilities associated with Fermi surface nesting, the classical examples being α-U and Cr. Whereas α-U displays a strong Kohn anomaly in the phonon spectrum that ultimately leads to the formation of charge density waves (CDWs), Cr is known for its nesting-induced spin density waves (SDWs). Recently, it has become clear that a pronounced Kohn anomaly and the corresponding softening in the elastic constants is also the key factor that controls structural transformations and mechanical properties in compressed group VB metals—materials with relatively high superconducting critical temperatures. This article reviews the current understanding of the structural and mechanical behavior of these metals under pressure with an introduction to the concept of the Kohn anomaly and how it is related to the important concept of Peierls instability. We review both experimental and theoretical results showing different manifestations of the Kohn anomaly in the transverse acoustic phonon mode TA ($\xi 00$) in V, Nb, and Ta. Specifically, in V the anomaly triggers a structural transition to a rhombohedral phase, whereas in Nb and Ta it leads to an anomalous reduction in yield strength.

Keywords: Kohn anomaly; Fermi surface nesting; phonon softening

1. Introduction

In 1959 Walter Kohn discovered [1] that in metallic systems the phonon spectrum $\omega(q)$ exhibits singularities or anomalies associated with the existence of the sharp Fermi surface (FS). In a hypothetical metal with a spherical FS, such anomalies in $\omega(q)$ would realize in the form of "wiggles" and come whenever $|\boldsymbol{q} \pm \boldsymbol{G}| = 2\boldsymbol{k}_F$, where k_F is the radius of the Fermi sphere and $\boldsymbol{G}$ is the reciprocal lattice vector [1,2]. These wiggles, or what we now call Kohn anomalies, are manifestations of the singularity in the electron response function $\chi(q)$ at $q = 2k_F$. The singularity reflects the qualitative change in the electronic screening due to electron–phonon coupling; for $q < 2k_F$, there are some zero-energy electron excitations, which are no longer possible for $q > 2k_F$. Within the model of ions immersed in and screened by a uniform electron gas, $\chi(q)$ reduces to the Lindhard response function, $\chi_0(q)$, whose first derivative logarithmically diverges at $q = 2k_F$, thus explaining the corresponding anomaly in $\omega(q)$ [2].

A Kohn anomaly is essentially what gives rise to fundamental instability in one-dimensional (1D) systems with a partly filled band. Peierls was the first to show that such systems are unstable

against generation of a charge density wave (CDW) with wave length $\lambda = \pi/k_F$ [3]. This instability takes place at any weak interaction of electrons with each other or with ions because in 1D not only the first derivative of $\chi_0(q)$ but also $\chi_0(q)$ itself logarithmically diverges at $q = 2k_F$. The gain in energy is maximal in the case of the half-filled band, for which $\lambda = 2a$, where a is the lattice constant of a 1D chain, and the new lattice period is doubled compared with the initial lattice constant a [3]. There are many real materials which can be considered as quasi-1D and are consistent with the Peierls–Kohn picture; they exhibit giant Kohn anomalies and undergo Peierls transitions to an insulating state at relatively low temperatures. Examples include tetrathiafulvene-tetracyanoquinodimethan or TTF-TCNQ-based charge-transfer salts and square planar complexes of the mixed-valence metals (Pt, Ir) [4,5].

In simple 3D metals, like Al and Pb, Kohn anomalies are weak and do not cause any lattice instability [2]. However, even in 3D metallic systems, anomalies can acquire an enhanced character and manifest themselves not as "innocent" wiggles, but as strong kinks and dips capable of driving lattice distortions. Such an enhancement comes from so-called "nesting": the existence of two patches of the FS which are identical in shape and are separated by a (nesting) vector $\boldsymbol{q}_n$ [6–9]. There are electronic transitions with the momentum transfer $\boldsymbol{q}_n$ that lead to the "enhanced Kohn anomaly". The nesting portions of the FS can belong to the same sheet (self or intraband nesting) or different sheets (interband nesting). In order to realize a "good self-nesting", the corresponding sheet of the FS should contain finite cylindrical or flat regions [7,8]. For a "good interband nesting", the two relevant FS sheets (i and j) should contain regions that coincide in shape and size [9].

The previously mentioned geometric features of the FS are only *necessary* but not sufficient conditions for the realization of the "enhanced Kohn anomaly", despite the fact that they lead to a sharp peak (divergence) in the imaginary part of the noninteracting susceptibility, Im $\chi_0(q)$, which literally shows FS nesting [10,11]. The quantity that is really responsible for strong Kohn anomalies and CDW ordering is the real part, Re $\chi_0(q)$ [10]. For a strong peak in Re $\chi_0(q)$, an additional constraint on the velocities of the states $\varepsilon_i(\boldsymbol{k})$ and $\varepsilon_j(\boldsymbol{k} + \boldsymbol{q_n})$ connected by $\boldsymbol{q}_n$ is required—they should be antiparallel and nearly equal in magnitude [11]. This is the reason why many researchers use "nesting" to mean the condition $\varepsilon_i(\boldsymbol{k}) = -\varepsilon_j(\boldsymbol{k} + \boldsymbol{q_n})$, where $\varepsilon_i(\boldsymbol{k})$ is the electron spectrum measured relative to the Fermi level. Such a condition is sufficient for a peak in Re $\chi_0(q)$ since it automatically imposes the opposite velocities on the nested portions of the FS. In some semimetals this condition is satisfied in a wide range of energies around the Fermi level, especially in cases when they have electron and hole FSs of the same shape and size. Such semimetals are usually unstable against the formation of indirect band-gap ("excitonic") semiconductors, which can be in either a CDW or SDW (spin density wave) state, whereby $\boldsymbol{q}_n$ becomes the superstructural vector [9,12–14].

Recently, much attention has been given to the layered transition dichalcogenides 2H–$NbSe_2$ and 2H–$TaSe_2$. These systems were commonly considered to be *classical* Peierls systems since their discovery in the early 1970s [5,10,11,15,16]. It has come as a surprise that in these systems the imaginary part of noninteracting susceptibility, Im $\chi_0(q)$, in the constant matrix element approximation, peaks at the vector $\boldsymbol{q}$ = (1/3,1/3,0), which does not coincide with the CDW wavevector, $\boldsymbol{Q_{CDW}}$ = (1/3,0,0) [10,11]. At the same time, the real part, Re $\chi_0(q)$, exhibits a very weak peak near $\boldsymbol{Q_{CDW}}$. All these results suggest that CDWs in 2H–$NbSe_2$ and 2H–$TaSe_2$ are not nesting derived [5,10,11]. Explicit inclusion of the matrix elements in the noninteracting electronic susceptibility, $\chi_0(q, \omega)$, does not change this conclusion qualitatively [15]. Moreover, due to their strong q-dependence, the matrix elements further weaken the manifestation of the FS nesting in the resulting $\chi_0(q, \omega)$. Keeping in mind that $\boldsymbol{Q_{CDW}}$ in 2H–$TaSe_2$ is not related to the FS nesting, Gor'kov suggested an original theory of CDW transformation in this and similar systems [16]. According to this theory, strong electron–phonon interactions tightly bind ions and electrons together, in a nonadiabatic manner. As a result, the ions move in effective double-well potential. At a low-enough temperature, they become trapped by one of the two minima; this corresponds to a formation of a CDW.

Strong Kohn anomalies and associated lattice instabilities have been observed only in few pure metals (i.e., in α-U [17,18]). Indeed, α-U is the only element in the periodic table which exhibits CDW

instability. Uranium metal undergoes three temperature-driven phase transitions in the temperature interval 47 K to 30 K. These three phases are called α_1, α_2, and α_3 [17]. The first phase transition, α_1, "doubles" the unit cell in the x-direction; the second phase transition, α_2, makes the unit cell six times larger in the y-direction; the third phase transition, α_3, makes the unit cell 27 times larger in the z-direction, resulting in the transformation of uranium to the element with the primitive cell which has a volume of ~6000 Å^3 [17]. Fast et al. [19] have shown that the α_1 structure can be viewed as a phonon (Σ_3) distortion of the ordinary α-U structure which is driven by the change of the FS topology: the part of the FS affected by a Peierls-like distortion shows a strong nesting of the narrow f-band in the x-direction. Fast et al. [19] have also shown that the FS nesting in the y-direction, which occurs upon cooling of the α_1 structure, causes slight modification of the α_1 structure and creation of the α_2 phase.

In systems with relatively strong exchange electron–electron interaction, FS nesting can lead to a strong Kohn anomaly in the spin wave rather than the phonon spectrum. If strong enough, such an anomaly can trigger the formation of spin density waves (SDWs). This is the case for chromium [20]. In nonmagnetic Cr, there is a good nesting between two extended FS pockets—the N-centered hole pocket and Γ-centered electronic pocket. The corresponding nesting vector $\boldsymbol{q}_n$ almost coincides with (1/2,0,0) and explains the antiferromagnetic ordering in Cr at relatively low temperatures.

Although very rare in pure metals, strong Kohn anomalies have been observed in several metallic alloys including the so-called "shape memory" alloys such as NiTi [8]. In these alloys, as the temperature decreases and approaches the martensitic transformation point M_s, a number of the so-called "premartensitic" phenomena occur, including the softening of the phonon modes and formation of the intermediate (often incommensurate) phases [8]. At this point, the unambiguous connection between the FS nesting, phonon dips, and premartensitic modulated structures is well established for NiTi [21,22], Ni_2MnGa [23–27], Ni-Al, [28–30], AuCd [31], CuZn [32], $AuCuZn_2$, [32], and other shape memory alloys. In the case of Ni-Al, for example, the calculations perfectly explain the experimentally observed shift of the phonon anomaly as a function of both composition and uniaxial squeezing [29].

Another class of alloys, whose lattice stability is defined by the nesting properties of the FS, are the noble-metal-based alloys such as CuAu, Cu_3Au, Au_3Cu, Cu_3Pd, Cu_3Pt, Ag_3Mg, Al_3Ti, etc., [33–36]. These alloys are unstable against the formation of the long-period superstructures (LPSs); both 1D and 2D and both incommensurate and commensurate. It has been discovered that 1D LPSs are caused by Peierls instability associated with flat (nesting) patches on the FS divided by the vector $2\boldsymbol{k}_F$ at which Re $\chi_0(q)$ peaks [33,35,36]. Lifting of this instability is accompanied by the formation of LPSs with the period $2\boldsymbol{M} = \pi/|\boldsymbol{k}_F|$. It is remarkable that this theory is also able to explain rather exotic 2D LPSs with substantially different periods $2\boldsymbol{M}_1$ and $2\boldsymbol{M}_2$ in two mutually orthogonal directions. Such LPSs stem from the two different nestings characterized by vectors $\boldsymbol{D}_1$ and $\boldsymbol{D}_2$, such that $2\boldsymbol{M}_1 = 2\pi/|\boldsymbol{D}_1|$, and $2\boldsymbol{M}_2 = 2\pi/|\boldsymbol{D}_2|$ [34].

Graphene appears among the truly 2D materials demonstrating strong Kohn anomalies. In graphene, the conduction and valence bands touch each other in a linear fashion at two inequivalent Dirac points, $\boldsymbol{K}$ and $\boldsymbol{K}'$, connected by time-reversal symmetry. Graphene is characterized by good nesting between the valence and conduction bands, which can be expressed as $\varepsilon_\iota(\boldsymbol{k}) = -\varepsilon_j(\boldsymbol{k})$ or $\varepsilon_\iota(\boldsymbol{k}) = -\varepsilon_j(\boldsymbol{k} + \boldsymbol{K} - \boldsymbol{K}')$, where the $\boldsymbol{k}$ vector is measured relative to a Dirac point and the valence (i) and conduction (j) band energies are measured relative to the Fermi level [37]. Since the difference $\boldsymbol{K} - \boldsymbol{K}'$ is again a Dirac point, the anomalies in phonon spectra $\omega(q)$ occur at $\boldsymbol{q} = 0$ (the Γ point) or $\boldsymbol{q} = \boldsymbol{K}$. Such anomalies manifest themselves as sharp kinks and have been observed in quasi-freestanding graphene, namely, in the in-plane optical phonons at $\boldsymbol{q} = \boldsymbol{\Gamma}$ (LO branch) and $\boldsymbol{q} = \boldsymbol{K}$ (TO branch) [38,39]. In 2D hydrogenic honeycomb lattice or H-graphene, Kohn anomalies are so strong that they can trigger 2D Peierls-like distortions leading to a $\sqrt{3} \times \sqrt{3}$ superstructure [37].

From general considerations it is clear that even the weak Kohn anomaly becomes *critical* if the corresponding nesting vector $\boldsymbol{q}_n$ shrinks and collapses to zero. In such a case the relevant soft mode can freeze in directly or force the elastic constants to soften to such a degree that they will initiate

structural transformation. Below we show that this is what happens in the group of VB transition metals under pressure. These metals are also interesting in the sense that until recently they have not been expected to exhibit any instability related to FS nesting.

2. FS Nesting and Kohn Anomaly in V, Nb, and Ta

2.1. Early Search for Phase Transformations in V, Nb, and Ta

During the past 20 years, the group VB transition elements (vanadium, niobium, and tantalum) have been the subject of numerous experimental and theoretical studies [40–92]. Their superconducting properties (for example, Nb has the highest critical transition temperature T_c = 9.5 K among the elemental metals [89]) and unique refractive mechanical properties at extreme temperatures place these metals in the position of basic building blocks of intermetallic compounds. Struzhkin et al. [40] have studied the superconducting transition temperature of niobium at pressures up to 1.32 Mbar. They found anomalies in $T_c(p)$ at 50–60 kbar and 600–700 kbar and suggested that these anomalies originate from an electronic topological transition (ETT). Takemura and Singh [57] have performed X-ray diffraction (XRD) measurements at ambient temperature. They suggest that niobium remains in the ambient pressure BCC structure at pressures up to at least 1.45 Mbar. Later, Ostanin et al. [45] and Tse et al. [53] performed a theoretical investigation of the electron–phonon coupling in high-pressure Nb and found two different ETTs that are responsible for these anomalies.

For Ta (which remains an ambient pressure BCC structure up to 1.74 Mbar [42,43]), T_c changes little from the ambient pressure value of 4.4 K to 450 kbar with the absence of the ETT proposed for Nb by Struzhkin et al. [40]. It is worth mentioning that Diamond Anvil Cell (DAC) measurements by Weir et al. [42] (the pressure gradient method) have not found any softening in the yield stress up to 1 Mbar pressure.

Ishizuka et al. [46] have conducted DAC experiments on vanadium at pressures up to 1.2 Mbar. They found that T_c = 5.3 K at equilibrium pressure and T_c increases linearly with pressure and reaches 17.2 K at 1.2 Mbar. In addition, Ishizuka et al. [46] have also identified a small step-like increment in T_c near 600 kbar. Takemura [44] has performed high-pressure DAC powder XRD measurements on vanadium and niobium which showed no anomalies in the equations of state (EOS) that can be attributed to the ETT up to the maximum pressure of 1.54 Mbar. Louis and Iyakutti [51] have computed the electronic structure, total energy, and superconductivity of vanadium under pressure. At ambient pressure, the calculated value of T_c is 5.98 K, which is in a good agreement with the observation by Ishizuka et al. [46] (T_c = 5.3 K) and, at 1.2 Mbar, the calculated value of T_c = 18.21 K which is close the experimental value of T_c = 17.2 K reported by Ishizuka et al. [46] at the same pressure. The calculations by Louis and Iyakutti [51] predicted phase transformation from the ambient pressure BCC structure to a simple cubic (SC) structure at p ~1.393 Mbar with estimated T_c ~20.99 K at the transition pressure. A metastable body-centered tetragonal (BCT) phase in vanadium has been predicted by Nnolim et al. [52]

2.2. Fermi Surface Nesting and Pre-Martensitic Softening in V, Nb, and Ta at High Pressures

In order to investigate structural phase transition from the BCC to another structure, Suzuki and Otani [49,61] calculated the lattice dynamics of vanadium in the pressure range up to 1.5 Mbar. They discovered that the transverse acoustic phonon mode TA ($\xi 00$), around ξ = 1/4, shows a drastic softening under compression and becomes imaginary at pressures above ~1.3 Mbar, suggesting an opportunity for structural phase transition. In the limit of short q-vector lengths ($q \to 0$), this mode is directly related to the trigonal shear elastic constant (C_{44}), so clear understanding of the anomaly in the TA curve is fundamentally important in the problem of the shear lattice stability of BCC vanadium. Suzuki and Otani [49,61], however, did not discuss the physical reasons behind the dip in the TA curve. The existence of the Kohn anomaly in the TA ($\xi 00$) of V around ξ = 1/4 was subsequently

confirmed by independent DFT calculations performed by Luo et al. [63], Krasil'nikov et al. [82,87], and Zhang et al. [86].

The synchrotron XRD measurements on vanadium by Ding et al. [62] suggest a new rhombohedral (Rh) phase around 640–690 kbar that is in the same pressure range where a small step-like increment in T_c was reported by Ishizuka et al. [46]. The BCC $\rightarrow$ Rh transition in V has been reported as a second-order phase transformation [62]. Later ab initio studies confirmed this discovery, suggesting that vanadium returns to the BCC phase in the pressure range of 2.5–3.2 Mbar [63,64,67–69]. Vekilov and Krasil'nikov [72] have concluded that, according to the Landau theory of phase transitions [93], the experimentally observed pressure-induced cubic $\rightarrow$ rhombohedral transition in vanadium [62] corresponds to the lattice losing its stability against C_{44} shear deformation. Bondarenko et al. [74] and Krasil'nikov et al. [78] have shown that, although the BCC $\rightarrow$ Rh phase transition in vanadium under compression is a first-order phase transition, the volume changes due to the lattice rearrangement $\Delta V/V_0 \leq 10^{-5}$ are negligibly small and the phase transition is close to a second-order phase transition. Krasil'nikov et al. [78] have mentioned that the BCC $\rightarrow$ Rh transition in vanadium is activated upon uniform deformation of the cubic structure. As a result, the transition to a new state with a lower symmetry (rhombohedral) than that of the initial state (cubic) takes place. The number of atoms in the unit cell of a crystal remains constant, and the point group of the low-symmetry phase is a subgroup of the point group on the initial structure. These transitions are referred to as elastic-phase transitions, and the critical phenomena during this kind of transitions are strongly suppressed. That is why in analysis of these structural transformations one can use the Landau theory of phase transition [93] with the deformation tensor of components as the order parameter.

Jenei et al. [77] have discovered an expression of the transition pressure from the cubic to rhombohedral structure as a function of the hydrostatic condition of the pressure media. Nonhydrostatic pressure leads to a lower transition point (~300 kbar), while in the case of quasihydrostatic compression in neon pressure medium, the BCC $\rightarrow$ Rh phase transition occurs at much higher pressure (~600 kbar). Antonangeli et al. [91] have recently applied inelastic X-ray scattering to investigate the phonon dispersion of the single-crystal V as a function of compression up to 450 kbar. These experiments found an unusual high-pressure behavior of the TA mode along the (100) direction and softening of the trigonal elastic constant C_{44} that triggers a rhombohedral lattice distortion occurring between 340 and 390 kbar. The measured compression (V/V_0) curve for vanadium followed the EOS for the BCC phase [62] up to 340 kbar, whereas a deviation is detected starting from 360 kbar. The volume discontinuity (~2%) due to the BCC $\rightarrow$ Rh transition, found by Antonangeli et al. [91], was not noted in previous studies by Ding et al. [62] and Jenei et al. [77] where measurements were performed on powders. Experiments by Antonangeli et al. [91] back up the first-order origin of phase transformation in accordance with group theory which indicates that BCC $\rightarrow$ Rh transitions are necessarily of the first order [82]. As was mentioned by Antonangeli et al. [91], the origin of the rhombohedral deformation between 340 and 390 kbar disagrees with XRD measurements by Ding et al. [62] (640–2690 kbar) but remains consistent with recent diffraction results by Jenei et al. [77] (300 kbar in nonhydrostatic conditions). The measurements of Antonangeli et al. [91] have been performed on comparatively big single crystals, which are more susceptible to nonhydrostaticity than powders.

The phonon anomaly in the TA ($\xi 00$) phonon branch of V was attributed to the existence of parallel parts of the FS which causes a strong electronic response at the nesting wave vector that translates these pieces one onto the other [59]. They also discovered that the nesting vector, q_n, spanning two flat pieces of the FS in the third band, already exists at ambient pressure and leads to the Kohn anomaly in the TA ($\xi 00$) phonon mode for small $q_n \approx 0.24(2\pi/a)$, where a is the lattice parameter. Since in the hydrodynamic limit ($q \rightarrow 0$) the trigonal shear elastic modulus C_{44} is connected to the TA ($\xi 00$) phonons, $\omega(q)$, by a simple relation so that $\rho\omega^2(q)/q^2 \rightarrow C_{44}$, the Kohn anomaly also softens this elastic modulus making it negative at pressures 1.80–2.75 Mbar. The full potential linear muffin-tin orbital [60] and projector augmented wave [69] calculations revealed the lower pressure limit of the BCC instability interval as 1.2 and 0.8 Mbar, respectively. According to Verma and Modak [67],

the BCC → Rh transition in V under pressure could happen even before the trigonal shear elastic modulus turns negative. A similar conclusion was independently derived by Luo et al. [63].

Using density functional theory (DFT), Lee et al. [64,65] have shown that the metastable Rh structure develops at 730 kbar and becomes the ground state (stable structure) at 840 kbar. Lee et al. [64] have called this rhombohedral phase "Rh1" with residual angle $\alpha = 110.25^{\circ}$. Lee et al. [64] have also predicted the development of a second metastable rhombohedral structure "Rh2" with residual angle $\alpha = 108.14^{\circ}$, which has not been seen experimentally, that becomes the ground state at 1.19 Mbar. As the pressure continue to increase, the ground state (Rh2) phase lastly reverses to the BCC structure (with the residual angle $\alpha = 109.47^{\circ}$) at 2.8 Mbar, and at 3.15 Mbar the BCC structure becomes the exclusive mechanically and thermodynamically stable structure. Lee et al. [64] have concluded that the BCC → Rh transition is of first order with a very small latent heat of transformation (much smaller than the thermal fluctuation at room temperature), which is in accord with the conclusions of Krasil'nikov et al. [82] and Antonangeli et al. [91] but contradicts the second-order transition suggested by Ding et al. [62]. Lee et al. [65] have performed DFT calculations of the elastic constants of vanadium in four structure modifications BCC → Rh1 → Rh2 → BCC as a function of compression. The calculated elastic constants have been used to determine the polycrystalline shear modulus as a function of compression. Rudd and Klepeis [66] have used these results to construct the multiphase Steinberg–Guinan model for vanadium. According to refs [65,66], the shear modulus of polycrystalline vanadium has been found to increase up to ~400 kbar and then to decrease with a further increase in compression up to ~1.20 Mbar. Lee et al. [65] have also shown that the volume change associated with above-mentioned phase transition in vanadium under compression is very small (no more than 0.15%), which is in accord with conclusions of Bondarenko et al. [74] and Krasil'nikov et al. [75]. This makes it very difficult to establish the order (first or second) of these phase transformations.

The prediction of the two high-pressure rhombohedral phases (Rh1 and Rh2) in V is supported by alternative DFT phonon spectra computations by Luo et al. [63].

Klepeis et al. [75] have performed DAC measurements of the yield strength of vanadium up to 900 kbar. The yield strength (the critical stress required to achieve a plastic deformation in a metal) largely depends on the shear elastic constant [47]. Unconventional softening of the shear modulus should influence the yield strength and other mechanical properties. Klepeis et al. [75] found that after an initial increase in the strength with compression, a decrease in the strength of V starts at ~400–500 kbar. Klepeis et al. [75] have attributed this unusual strength behavior to premartensitic softening of the shear modulus [65,66] associated with the BCC → Rh1 phase transformation induced by existence of a Kohn anomaly in the TA ($\xi 00$) phonon branch. Klepeis et al. [75] have stressed that the strength is *superelastic*: the magnitude of the rise and recede in strength is much greater than that of the shear modulus.

The BCC → Rh phase transformation on vanadium under compression has been detected by static synchrotron XRD DAC experiments [62,75,91]. Yu et al. [85] have performed shock experiments on vanadium measuring phase transformation discontinuity of the sound velocity against shock compression. The detected phase transformation from the BCC to the unknown phase has been detected at 605 kbar, which is in accord with both DAC measurements [62] and the first-principles calculations [64]. However, the measured shear modulus shows unusual behavior: it rises slightly with pressure from ambient to 320 kbar, and then declines with pressure before rising as the phase transition is approached at 605 kbar. Yu et al. [85] have argued that the proposed BCC → Rh phase transformation in vanadium under shock compression can start at 320 kbar and ends at 605 kbar, which is in accord with the DAC experiment of Jenei et al. [77]. However, in contrast with the results from DAC measurements [75] and theoretical work [66], the shear modulus and yield strength measured by Yu et al. [85] show abrupt rise at around the upper border of the phase transformation, at 605 kbar.

Qiu and Marcus [68] have also performed ab initio calculations of the phase transformations in vanadium under compression. They confirmed the existence of two rhombohedral phases, Rh1 and Rh2, and that pressure induces structural transformations in the sequence BCC → Rh1 → Rh2 → BCC discovered by Lee et al. [64]. However, they also found one significant inconsistency in the exact values

of the transition pressure. One of the most noticeable differences presented by Qiu and Marcus [68] was that the BCC → Rh1 transition pressure occurs at 320 kbar, which is much smaller than all other theoretical predictions. One should mention that all calculations, including those by Qiu and Marcus [68], have been performed under hydrostatic conditions and, thus, are inappropriate for Jenei et al.'s [77] argument (nonhydrostaticity). To verify the reason for the discrepancy between calculations by Lee et al. [64] and Qiu and Marcus [68], Wang et al. [90] have performed identical calculations to that of Lee et al. [64] but additionally optimized the structures. Wang et al. [90] have selected Rh1 and Rh2 as the starting structures and optimized them at different pressures. The calculated enthalpy difference with respect to the BCC phase together with the variation of the structural parameter (the residual angle α) in the Rh1 and Rh2 structures as a function of pressure are shown in Figure 1 (taken from [90]). According to Wang et al. [90], the results of fully relaxed calculations reveal that the BCC → Rh1 transition does not occur at 300 kbar as was suggested by Jenei et al. [77]. The metastable region of the Rh1 phase exists up to 500 kbar, but at lower pressures the Rh1 phase remains highly unstable. Wang et al. [90] have indicated that relaxation of the Rh1 phase to the BCC phase is far from perfect. The residual angle α is approximately 109.51° at 200–400 kbar. This reflects the fact that nonhydrostatic loading can drive vanadium towards rhombohedral-like deformations. Wang et al. [90] have indicated that the residual angle measured by Jenei et al. [77], α = 109.61°, is far smaller than Lee et al.'s computed value of α = 110.25° [64], but very close to their calculated *imperfect* BCC value, α = 109.51°, that collapses from the Rh1 phase as shown in Figure 1. Wang et al. [90] have also mentioned that another rhombohedral phase (Rh2) converts to a similar distorted BCC structure only with the residual angle α = 109.39° at pressures less than 1.1 Mbar. According to Wang et al. [90], the Rh1 phase becomes the ground state above 980 kbar. It has a larger residual angle, α = 110.17°, relative to the residual angle of the ideal BCC structure, α = 109.47°. Phase transformation to another rhombohedral phase (Rh2) occurs at ~1.28 Mbar, which reaches maximum stability at ~2.1 Mbar, with α = 108.23°. The Rh2 phase remains the ground state up to ~2.84 Mbar. As compression increases, the Rh2 phase becomes the metastable phase and finally collapses to the BCC phase at ~3.0 Mbar. The metastability of the Rh1 structure reaches up to ~2.47 Mbar, where it also converts back to the BCC phase. Wang et al. [90] have concluded that their results are in a good agreement with results of Lee et al. [64]. This means that Lee et al.'s [64] approach is consistent with the full structural relaxation calculations.

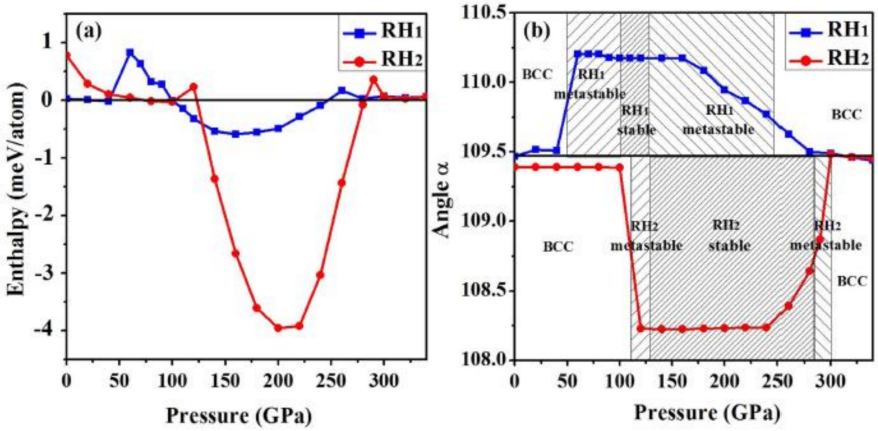

Figure 1. (**a**) Enthalpy difference of vanadium in Rh1 and Rh2 structures at zero Kelvin with respect to the BCC phase as a function of pressure. (**b**) Variation of the residual angle α in Rh1 and Rh2 structures as a function of pressure at zero Kelvin. Note that α = 109.47° corresponds to the perfect BCC structure and 1 GPa = 10 kbar.

Calculations [59,60,64,65,67,90] assume that the unit cell volume is conserved. As was shown by Le et al. [64] and Wang et al. [90], the total energy along the deformation path can be corrected from

an internal energy, E, to an enthalpy, H, to study phase equilibrium at constant pressure. For a small distortion δ, the enthalpy at pressure $p_0 = p(\delta = 0, V_0)$ may be corrected to a good approximation from the internal energy using the formula [64,90]

$$H(\delta, p_0) \approx E(\delta, p_0) + p_0 V_0 - \frac{1}{2B(\delta, V_0)} \Delta p(\delta, V_0)^2 V_0$$

where $\Delta p(\delta, V_0) = p(\delta, V_0) - p_0$ is the pressure change at the fixed volume V_0 due to the rhombohedral deformation δ and $B(V_0)$ is the bulk modulus at the fixed volume. According to refs [64,90], the corrections from the third term are extremely small and, as a result, the internal energy $E(\delta, p_0)$ is sufficient to study phase equilibrium. Qiu and Marcus [68] have disputed that this treatment could cause a higher transition pressure in Lee et al.'s [64] calculations. Taking into consideration that the results of 'unrelaxed' calculations by Lee et al. [64] are in a good accord with the full structural relaxation calculations by Wang et al. [90], one can conclude that the justification by Qiu and Marcus [68] cannot interpret the small value of the BCC → Rh1 transition pressure, 320 kbar, obtained by Qiu and Marcus [68], in comparison with results of Lee et al. [64], 840 kbar, or Wang et al. [90], 980 kbar.

As was mentioned above, instability of the BCC phase of vanadium under compression appears to be associated with a pressure-induced substantial softening of the shear elastic constant C_{44} [61,66,67]. In fact, vanadium's group VB relatives—niobium and tantalum—also show a similar but less-pronounced softening of C_{44} (see Figure 2). For vanadium, C_{44} initially increases with pressure but as pressure reaches ~200 kbar, C_{44} dramatically decreases. Landa et al. [71] have predicted the BCC → Rh phase transition at 600 kbar, close to the observed 600–700 kbar [62]. For Nb, a similar behavior is observed with the shear constant reaching a low minimum close to 500 kbar before rising again. In Ta, the softening is less severe but apparent between 500 and 800 kbar.

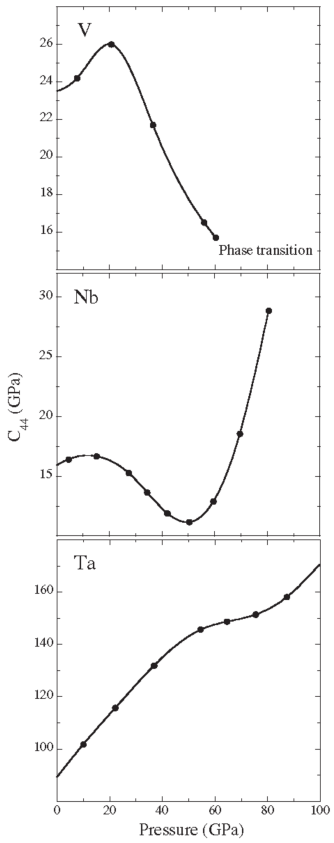

Figure 2. Calculated pressure dependence of the shear elastic constant in BCC V, Nb, and Ta [71]. Note that 1 GPa = 10 kbar.

With the X-ray scattering approach, Bosak et al. [70] have discovered several anomalies in the phonon dispersion curve for V along high-symmetry directions. One of them was an upward bending of the TA phonon mode along the Γ-H direction, ($\xi 00$), around $\xi = 0.24$—this anomaly was predicted in refs [49,61]. From inelastic neutron scattering, Nakagawa and Woods [94] have discovered a decrease in TA ($\xi 00$) phonon frequencies for niobium around $\xi = 0.20$ (compared to $\xi = 0.24$ for V). Woods [95] has conducted frequency–wave–vector dispersion relation experiments in tantalum using an inelastic neutron scattering technique similar to that for niobium [94]. His measurements indicated strong analogies with niobium, measured earlier [94]; however, a dramatic decrease below the elastic constant line for the TA ($\xi 00$) phonon mode, found for Nb by Nakagawa and Woods [94], was not detected.

Whether the TA ($\xi 00$) phonon anomaly in VB transition metals is actually electronic and related with "nesting areas" of the FS can be resolved by comparing the nesting vectors, $\boldsymbol{q_n} = 2\boldsymbol{k_F}$, in all the VB metals with the locations of their phonon anomalies, measured experimentally: V [70], Nb [94], and Ta [95]. As mentioned in the introduction, the vectors $\boldsymbol{q_n}$ should correspond to peaks in the real part of the noninteracting susceptibility, Re $\chi_0(q)$, which hereafter will be denoted simply as $\chi(q)$. Therefore, if the positions of some phonon anomalies of a metal system are closely correlated with the positions of maxima in $\chi(q)$, this would strongly indicate that these anomalies are of the Kohn nature.

Figure 3 shows the partial (associated with the third band only, see [59,60] for details) contribution to the generalized susceptibility, $\chi(q)$, of V, Nb, and Ta calculated along the Γ-H ($\xi 00$) direction at ambient pressure by Landa et al. [76]. As can be seen from this plot, the generalized susceptibility has a peak (due to the intraband nesting [59,60]) at $\xi \approx 0.24$, 0.16, and 0.28 for V, Nb, and Ta, respectively, marking the location where the Kohn anomaly on the TA ($\xi 00$) phonon curve is likely to exist. It is obvious that this peak is more significant for V and Nb than for Ta. This suggests that the Kohn anomaly is weaker in Ta than in V and Nb. To validate this conclusion, Landa et al. [76] show in Figure 4a–c the experimental phonon dispersion TA branches in the ($\xi 00$) direction for V, Nb, and Ta, respectively, using numerical data on the phonon frequencies from refs [70,94,95]. The position of the peak on the partial generalized susceptibility curve at equilibrium pressure, marked in Figure 3, is shown by an arrow in Figure 4. Obviously, the position of the calculated peak in $\chi(q)$ is in fair agreement with at the area of maximum deviation below the elastic constant line of the experimental TA ($\xi 00$) phonon branch. In relation to V, this deviation is observed to a larger extend for Nb and to a smaller extent for Nb and Ta.

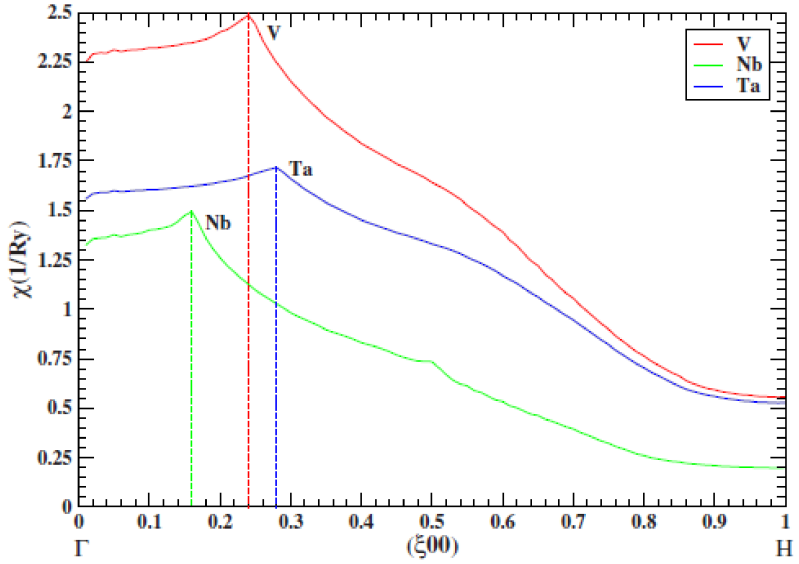

Figure 3. Partial (in the summation over bands, only the third band is included) electron susceptibility of V, Nb, and Ta calculated along the Γ-H direction at ambient pressure [76].

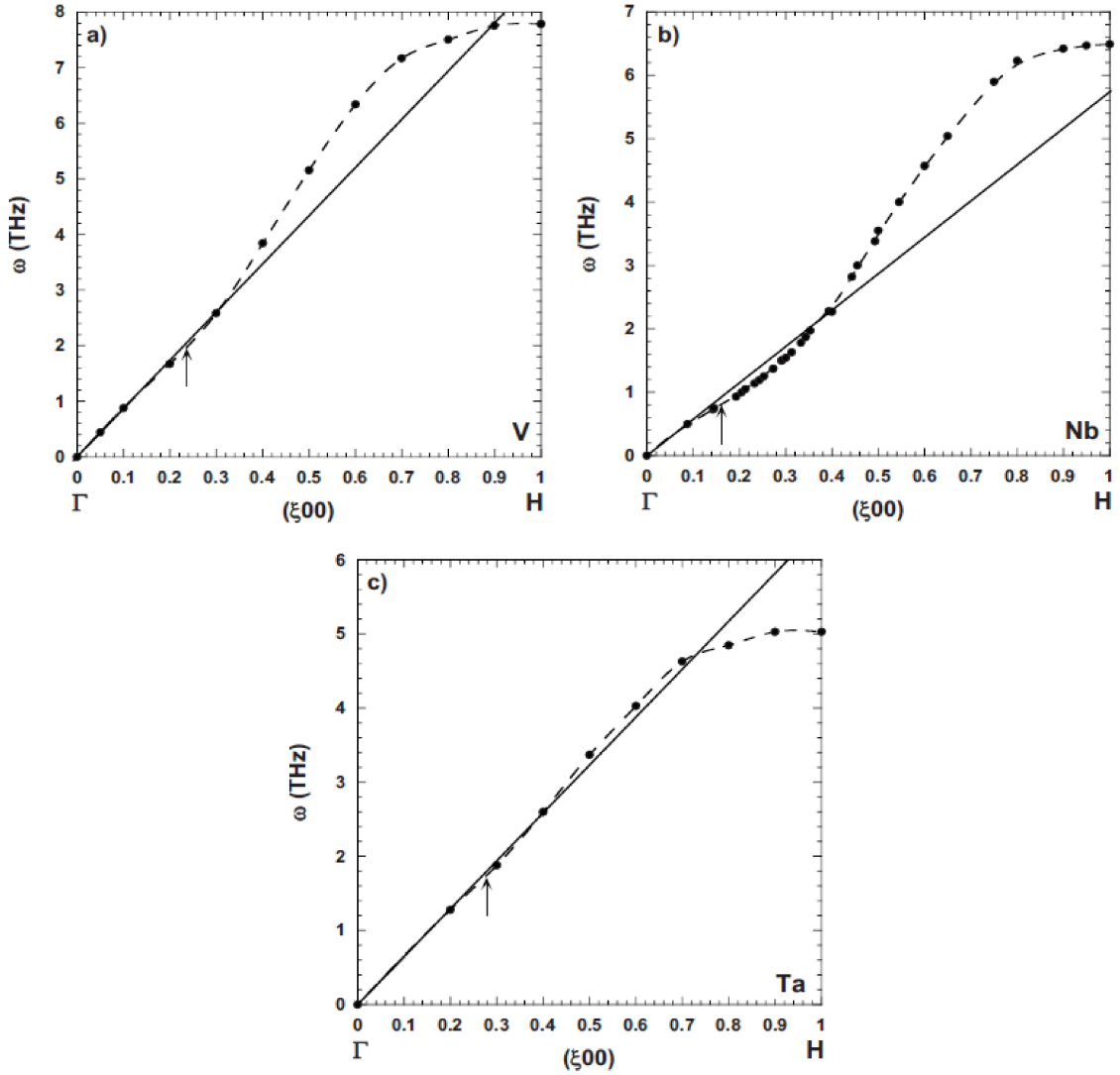

Figure 4. The experimental phonon dispersion TA curve in the ($\xi 00$) direction for (**a**) V [70,96], (**b**) Nb [97,98], and (**c**) Ta [95]. The arrow indicates the Kohn anomaly obtained from ab initio calculations [76]. The straight line represents the elastic constant line.

Tracing the pressure dependence of the position of the maximum on the generalized partial susceptibility, Landa et al. [76] plotted (Figure 5) the magnitude of the nesting vector, or the position of the Kohn anomaly, as a function of pressure. These calculations show that the nesting vector decreases as pressure increases and the termination of a so-called "jungle-gym" hole-tube occurs at 2.50, 0.75, and 2.75 Mbar for V, Nb, and Ta, respectively. This is in a good agreement with results of Koči et al. [69] for V and Nb, although their calculations revealed a lower termination pressure for Ta (~2.25 Mbar).

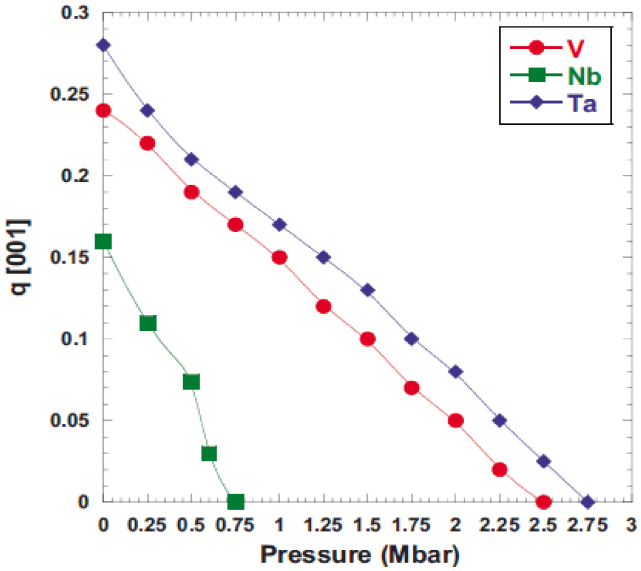

Figure 5. The magnitude of the nesting vector for V, Nb, and Ta as a function of pressure [76].

2.3. Strength and Elasticity of Nb and Ta

Reviewing the most recent publications on vanadium, let us discuss two remaining representatives of the group VB transition metals: Nb and Ta. The pressure–volume relationship of niobium has been investigated by Takemura [44] and Takemura and Singh [57], and they did not find any sign of discontinuity up to ~1.5 Mbar. This result suggests that niobium shows no structural transitions with substantial volume collapse in this pressure interval. Numerous calculations suggest that the BCC phase of Nb remains stable up to very high compression. Singh and Takemura [48], Singh and Lierman [80], and Ahuja et al. [99] have studied the strength and elasticity of Nb under high pressure. The compressive strength of Nb exhibits an anomalous variation between 0 and 150 kbar—it initially increases with pressure and exhibits a shallow maximum at ~50 kbar and then a minimum at ~120 kbar followed a monotonic increase at higher pressures (up to 400 kbar). As was mentioned above, Struzhkin et al. [40] have observed anomalies in the superconducting transition temperature T_c in Nb at 50–60 kbar and suggested that this anomaly arises from the ETT. Wang et al. [92] have also suggested that the ETT could be responsible for the unusual behavior of the compressive strength around 50–60 kbar.

Ab initio calculations by Koči et al. [69] significantly underestimated the value of the trigonal shear elastic constant C_{44} in Nb. Liu and Shang [79] performed DFT calculations of the electronic density of states (DOS) and the FS of Nb. They suggested that the most probable reason for C_{44} underestimation is related to the nesting features of the FS which produce a van Hove singularity in the electronic DOS close to the Fermi level. A similar situation in simultaneous manifestations of the 2D van Hove singularity and FS nesting has been discussed by Naumov and Velikokhatnyi [32] for β-NiAl alloys. Liu and Shang [81] have studied how alloying of Nb with other refractory metals (Ti, Zr, Hf, V, Ta, Cr, Mo, and W) influences it elastic properties. Their conclusion correlates with the most important result of Landa et al. [71] in which the phase stability of Group VB elemental metals was studied using DFT calculations. Alloying with a small part of a neighbor will stabilize or destabilize the BCC structure compared with the low-symmetry Rh structure. It was also shown that band-filling dictates the phase stability when a particular Group VB metal is alloyed with its nearest neighbors within the same column of the periodic table. Then, the neighbor with less or more *d* electrons, destabilizes and stabilizes the BCC structure, respectively. When alloying with neighbors of higher *d*-transition series, electrostatics dominates and stabilizes the BCC structure. This has been discussed in detail previously by Landa et al. [76].

Wang et al. [92] have recently predicted a novel anomaly softening in C_{44} of niobium between 2.75 Mbar and 4.0 Mbar. However, this softening is not related to the FS nesting in Nb, which terminated at 750 kbar [59,76], but originates purely from the ETT. Wang et al. [92] have emphasized that the significant magnitude of the softening leads to an impressive elastic anisotropy in both the shear and Young's moduli of Nb. At 600 kbar, the anisotropy on the shear elastic constant approaches a maximum.

Tantalum is often used for testing purposes, for study of yield strength, and for comparing theoretical predictions of elastic and plastic properties under extreme pressure and temperatures [41–43,50,54–56,58,73,83,84,87,88]. As was mentioned above, tantalum possesses the BCC structure at ambient conditions and this structure remains stable up to at least 1.74 Mbar [42,43]. Söderlind and Moriarty [41] have shown that tantalum is regarded as a good example for demonstrating the successful applications of DFT to the structural stability of the transition metal up to 10 Mbar—the calculated cold EOS for BCC Ta is in an acceptable agreement with DAC experiments up to 0.75 Mbar and with reduced shock data up to 2.3 Mbar. Gülseren and Cohen [50] and Orlikowski et al. [58] have extended these studies within a wide temperature range (up to 10,000 K). Dewaele et al. [54] have performed single-crystal XRD refinement of the EOS of tantalum up to 1.01 Mbar. Dewaele and Loubeyre [55] have studied the effect of high pressure up to 930 kbar on the yield strength of tantalum single crystals. Klepeis et al. [56] have predicted that tantalum should exhibit an anomaly in both tetragonal (C') and trigonal (C_{44}) shear moduli at high pressure in the range of 1.0 to 2.0 Mbar

Antonangeli et al. [73] have studied the elasticity of Ta at pressures above 1 Mbar. Inelastic X-ray scattering (IXS) experiments showed a decrease in the aggregate shear velocity in the 500–900 kbar interval with a normal pressure dependence above 1.20 Mbar. The calculations, performed by Antonangeli et al. [73], suggested that in tantalum, similar to predictions for vanadium and niobium, this anomalous behavior is likely due to the intraband FS leading to the ETT and a complementary TA phonon branch softening. Antonangeli et al. [73] have presented a description of the elastic–plastic phase transitions in terms of an anomalous behavior of the elastic modulus under compression above 1 Mbar pressure. Guerrero and Marucho [84] have utilized classical molecular dynamics (MD) to study the elastic–plastic transition under uniaxial stress in defect-free BCC tantalum crystals. They demonstrated that the nucleation of the defects at the time scale of MD is due to dynamical instabilities (soft phonons) along the [100] direction. These 'unstable' soft phonons produce defect nucleation growing on nanosecond timescales when resolved shear stress reaches a critical value. Guerrero and Marucho [84] have discovered that these dynamical instabilities (soft phonons) play a significant role in the elastic–plastic transition in BCC tantalum crystals.

Hu et al. [83] have performed sound velocity measurements of tantalum under shock compression in the 100 kbar–1.1 Mbar range. They have found a kink in the longitudinal sound velocity around 600 kbar and suggested that it is caused by a possible shock-induced phase transformation. However, this suggestion has been questioned by Jing et al. [88] who have recently performed XRD-DAC measurements of the yield strength in tantalum at ambient temperature and elevated pressures up to 1.01 Mbar pressure. A yield strength softening was detected between 520 and 840 kbar, which is independent of structural transformations, preferred orientation/texture, and pressure-induced material damage, whereas a standard trend is observed below 520 kbar and above 840 kbar. The initial pressure of the softening is in an agreement with previous IXS pressure gradient measurements [73] as well as the ab initio calculations [71] which have revealed a surprising softening of the shear modulus of tantalum between 500 and 800 kbar. Figure 6, which is taken from ref [88], shows that the trigonal shear elastic modulus C_{44} (Figure 6a) determined either by first-principles calculations [71] or deduced from the measured sound velocity using the IXS technique [70] exhibits softening. Both yield strengths, calculated either using the shear modulus obtained using the Steinberg model [100] or that extracted from the IXS measurements [73] (Figure 6b)

also exhibit softening. The softening of the yield stress approximately follows the same trend as does the softening of the shear modulus deduced either by the first principles [71] or IXS measurements [73].

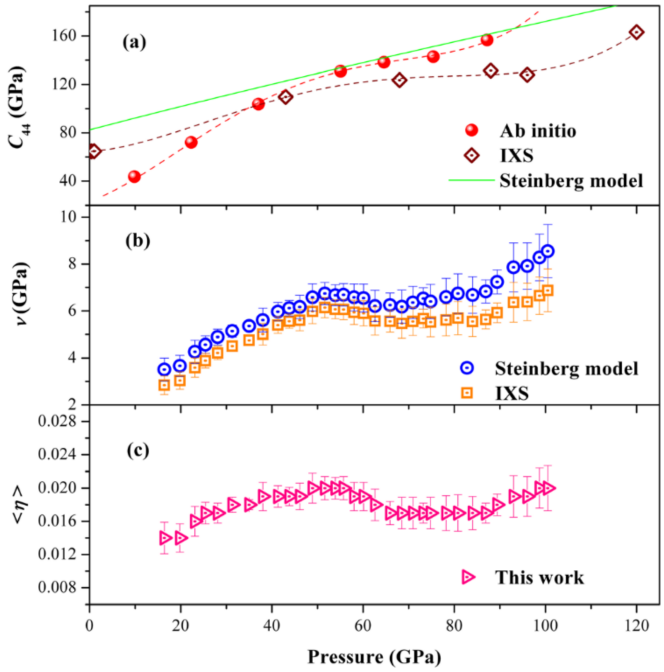

Figure 6. Pressure dependence of the shear modulus C_{44} (**a**); yield strength (**b**); and average microscopic deviatoric strain (η) (**c**) of Ta. The shear modulus C_{44} was predicted by theoretical calculations [71] (red dots), deduced from the sound velocity experimentally determined by IXS during DAC [73] (blue diamonds), and extrapolated from the Steinberg model [100] (solid line). Note that 1 GPa = 10 kbar.

3. Discussion

The chemical bonding of the elemental transition metals was believed to be well understood as originating from a gradual occupation of first bonding and later antibonding states as one proceeds through the transition series [101]. This scenario clearly explains the parabolic behavior in the atomic density and compressibility that reach a maximum at the maximum of filled bonding states near the center of the series. The known sequence of hexagonal close-packed (HCP), body-centered cubic (BCC), and face-centered cubic (FCC) phases in the *d*-transition metals is due to the population and specific form of the *d*-band electron density of states [102,103]. For the 3*d* transition metals, this sequence is slightly changed due to magnetism that differentiates bands of opposite spin [104]. Thus, for Group VB (V, NB, Nb), VIB (Cr, Mo, W), and for Fe (magnetic), the BCC phase exists because of their specific *d*-band occupation.

Recently, experimental studies on vanadium raised some doubts about the above-mentioned conventional view of bonding in the transition metals. Particularly, a new rhombohedral phase (Rh) has been found in the pressure range of 600–700 kbar by synchrotron XRD measurements [62,77,91]. DFT studies confirmed this discovery and suggested that vanadium returns to the BCC phase above approximately 3.0 Mbar [63,64,67]. It has been suggested that the intraband FS nesting (Kohn anomaly) is responsible for this peculiar behavior [59,60]. Instability of the BCC phase also appears to be associated with a pressure-induced considerable softening of the trigonal shear elastic constant C_{44}. In fact, vanadium's Group VB relatives—niobium and tantalum—also show a similar but less-pronounced softening of C_{44} (Figure 2). As was pointed by Klepeis et al. [75], the pressure-induced structure BCC $\rightarrow$ Rh transformation in vanadium is one of the most common reasons for strength loss.

Although Nb and Ta do not undergo BCC $\rightarrow$ Rh phase transformation, the softening of the trigonal shear elastic constant, C_{44}, of these metals causes significant softening of the yield strength at

high pressures. According to the soft-mode theory of the elastic–plastic phase transitions [105,106], the anomalous behavior of the elastic modulus under compression is essential in order to establish the fundamental relationship between the phonon dispersion and the yield strain (or the mechanism governing the defect generation in the perfect metallic crystal by the dynamical instabilities—the soft phonons [84]). Antonangeli et al. [73] mentioned that the topology of the electronic band structure near the Fermi level is identical for each of the group VB transition metals and causes the pressure-induced shear softening for Nb and Ta and the BCC → Rh transformation in vanadium. The effect, induced by the Kohn anomaly, is present in all group VB elements, but most noticeable in Period 4 (V), and decreases in magnitude to Period 6 (Ta) [73]. Only in the case of vanadium is the energy increase considerable enough to yield the BCC → Rh phase transition.

According to Figure 2, for niobium, C_{44} initially increases with compression, but close to 200 kbar it dramatically decreases, reaching a low minimum close to 600 kbar before rising again [68]. Wang et al. [92] have concluded that this anomalous behavior of the Nb shear modulus C_{44} in the pressure range 0–600 kbar mainly comes from the *underlying* Rh1 and Rh2 distortion and has the same softening mechanism which is observed in vanadium. According to Jing et al. [88], a similar hypothesis can be also applied to the softening of the shear modulus in tantalum.

Previous calculations by Landa et al. [60,71] show that a minimal (~3–5 at. %) part of 4*d*- (Zr, Nb, Mo) or 5*d*- (Hf, Ta, W) transition metal promotes the BCC phase of V at all compressions. Adding about 10 at. % of Cr to V also promotes the BCC phase at all compressions [64,71]. This investigation affirms that the Kohn anomaly (the FS nesting) and phonon (the shear modulus) softening can easily be suppressed by appropriate alloying. However, the compression-induced mechanical instability of BCC V, which results in formation of the rhombohedral phase close to 600–700 kbar at ambient temperature, will survive significant heating and compression [90,107]. Utilizing the self-consistent ab intio lattice dynamics approach, Landa et al. [107] have found that the Rh phase of vanadium remains stable under heating up to ~2500 K at early onset of the BCC → Rh transition (740 kbar). This temperature of destabilization (stabilization) of the Rh (BCC) phase is significantly below the shock melting temperature of BCC vanadium, T_m ~4000 K [108], as well as below the static (DAC) melting temperature, T_m ~ 2650 K [109]. According to Wang et al. [90], the electronic entropy decreases the temperature of the BCC phase recovery from the Rh phase: the Rh1 phase starts at 980 kbar (at ambient temperature) and remains stable below 1440 K and 1.4 Mbar; the stable region of the Rh2 phase is located between 1.26–2.80 Mbar with a maximum transition temperature of 1915 K at 2.11 Mbar.

As was mentioned in ref [107], the lattice vibrations at elevated temperatures promote recovery of the BCC structure of compressed vanadium at elevated temperatures. A similar mechanism of phase transformation (based on the vibrational entropy contribution to the Gibbs free energy) is appropriate for vanadium nitride (VN), which at ambient conditions exists in the rock-salt (B1) structure [110]. Kubel et al. [111] have found a cubic → tetragonal phase transition upon cooling bulk polycrystalline VN below 204 K. Wolf et al. [112] have predicted a dramatic decrease of the shear modulus C_{44} of VN in the B1 structure at about 1.2 Mbar compression which hints at possible mechanical instability. DFT calculations by Isaev et al. [113] and by Ivashchenko and Turchi [114] have revealed dynamic instabilities in VN in the B1 structure. These instabilities are characterized by imaginary phonon modes along the Γ-X direction at the *X* point at 0 K. Isaev et al. [113] have connected these peculiarities in the phonon spectra of VN to Kohn anomalies induced by the nesting of the FS. The schematic representation of a cubic → tetragonal phase transition in VN (the phonon dispersion curves with a distinct region of the imaginary frequencies and the related displacements of atoms) is offered by Řehák et al. [115] (Figure 5). Recently, Mei et al. [116] have utilized ab initio MD to prove that VN can be stabilized by anharmonic atomic vibrations in the B1 structure at ~250 K. Indeed, it has been discovered from XRD measurements by Kubel et al. [117] that, at room temperature, VN in the B1 structure is strongly anharmonic with atomic displacements randomly shuffled along the <111> crystallographic directions with respect to the ideal B1 lattice sites. These characteristics have been recently linked by Zheng et al. [118] to electron–phonon coupling effects in the VN lattice thermal conductivity.

In summary, we have shown how the concept of Kohn anomaly is related to phonon/electronic instability of the group VB transition metals upon compression and how this instability drives phase transformation in vanadium and leads to the anomaly reductions in the yield strengths of niobium and tantalum. This review paper covers a large quantity of experimental and theoretical research dedicated to the study of mechanical properties of these refractory metals over the last twenty years. Special attention is paid to the initial conception of Peierls instability, which traces back to 1930s, and which causes the FS nesting in the electronic structure, a sharp peak in Lindhard functions, Kohn anomaly in the phonon spectrum, and structural transformation in the lattice.

Acknowledgments: This work was performed under the auspices of the U.S. Department of Energy by Lawrence Livermore National Laboratory under Contract DE-AC52-07NA27344. I.I.N. support from DOE/NNSA award DE-NA-0002006 (CDAC), and DOE Office of Science, Office of Basic Energy Sciences Energy Frontier Research Center award DE-SC0001057 (EFree). L.V. acknowledges the Swedish Research Council, the Swedish Foundation for Strategic Research, the Swedish Foundation for International Cooperation in Research and Higher Education, and the Hungarian Scientific Research Fund (OTKA 109570).

Author Contributions: A.L., P.S. and I.I.N. wrote the paper. J.E.K. and L.V. wrote and corrected the paper.

Conflicts of Interest: The authors declare no conflict of interest.

References

1. Kohn, W. Image of the Fermi surface in the vibration spectrum of a metal. *Phys. Rev. Lett.* **1959**, *2*, 393–394. [CrossRef]
2. Woll, E.J.; Kohn, W. Images of the Fermi Surface in phonon spectra in metals. *Phys. Rev.* **1962**, *126*, 1693–1697. [CrossRef]
3. Peierls, R.E. *Quantum Theory of Solids*; Oxford University: New York, NY, USA, 1955.
4. Bulaevskii, L.N. Structural and superconducting properties of system with one-dimensional anisotropy. In *High-Temperature Superconductivity*; Ginzburg, V.L., Kirzhnits, D.A., Eds.; Consultants Bureau: New York, NY, USA; London, UK, 1982; pp. 241–281.
5. Zhu, X.; Guo, J.; Zhang, J.; Plummer, E.W. Misconceptions associated with the origin of charge density waves. *Adv. Phys. X* **2017**, *2*, 622–640. [CrossRef]
6. Taylor, P.L. Theory of Kohn anomalies in the phonon spectra of metals. *Phys. Rev.* **1963**, *131*, 1995–1999. [CrossRef]
7. Afanas'ev, A.M.; Kagan, Y. Singularities caused by electron-phonon interaction in the phonon dispersion law. *Sov. J. Exp. Theor. Phys.* **1963**, *16*, 1030–1034.
8. Katsnelson, M.I.; Naumov, I.I.; Trefilov, A.V. Singularities of the electronic anomalies of lattice properties in structure and pre-martensitic β-phases of metals and alloys. *Phase Trans.* **1994**, *49*, 143–191. [CrossRef]
9. Kopaev, Y.V. Possibility of an increase in the critical temperature as a result of a structural-transition-induced change in the electron spectrum. In *High-Temperature Superconductivity*; Ginzburg, V.L., Kirzhnits, D.A., Eds.; Consultants Bureau: New York, NY, USA; London, UK, 1982; pp. 179–211.
10. Johannes, M.D.; Mazin, I.I.; Howells, C.A. Fermi-surface nesting and the origin of the charge-density wave in $NbSe_2$. *Phys. Rev. B* **2006**, *73*, 205102. [CrossRef]
11. Johannes, M.D.; Mazin, I.I. Fermi surface nesting and the origin of charge density waves in metals. *Phys. Rev. B* **2008**, *77*, 165135. [CrossRef]
12. Keldysh, L.V.; Kopaev, Y. Possible instability of semimetallic state toward Coulomb interaction. *Sov. Phys. Solid State* **1965**, *6*, 2219–2224.
13. Halperin, B.I.; Rice, T.M. Possible anomalies at a semimetal-semiconductor transition. *Rev. Mod. Phys.* **1968**, *40*, 755–766. [CrossRef]
14. Barzykin, V.V.; Gor'kov, L.P. Ferromagnetism and superstructure in $Ca_{1-x}La_xB_6$. *Phys. Rev. Lett.* **2000**, *84*, 2207–2210. [CrossRef] [PubMed]
15. Faraggi, M.N.; Zubizarreta, X.; Arnau, A.; Silkin, V.M. On the stability of the electronic system in transition metal dichalcogenides. *J. Phys. Condens. Matter* **2016**, *28*, 184004. [CrossRef] [PubMed]
16. Gor'kov, L.P. Strong electron-lattice coupling as the mechanism behind charge density wave transformations in transition-metal dichalcogenides. *Phys. Rev. B* **2012**, *85*, 165142. [CrossRef]

17. Lander, G.H.; Fisher, E.S.; Bader, S.D. The solid-state properties of uranium a historical perspective and review. *Adv. Phys.* **1994**, *43*, 1–111. [CrossRef]
18. Marmeggi, J.C.; Currat, R.; Bouvet, A.; Lander, G.H. Phonon softening in alpha-uranium associated with the CDW transition. *Phys. B Condens. Matter* **1999**, *263–264*, 624–626. [CrossRef]
19. Fast, L.; Eriksson, O.; Johansson, B.; Wills, J.M.; Straub, G.; Roeder, H.; Nordström, L. Theoretical aspects of the charge density waves in uranium. *Phys. Rev. Lett.* **1998**, *81*, 2978–2981. [CrossRef]
20. Chan, S.-K.; Heine, V. Spin density wave and soft phonon mode from nesting Fermi surfaces. *J. Phys. F Met. Phys.* **1973**, *3*, 795–809. [CrossRef]
21. Zhao, G.-L.; Leung, T.C.; Harmon, B.N.; Keil, M.; Müllner, M.; Weber, W. Electronic origin of the intermediate phase of NiTi. *Phys. Rev. B* **1989**, *40*, 7999–8001. [CrossRef]
22. Naumov, I.I.; Velikokhatnyi, O.I.; Bashirov, V.Z. Charge density waves in B2 titanium compounds. *JETP Lett.* **1991**, *54*, 573–577.
23. Velikokhatnyi, O.I.; Naumov, I.I. Electronic structure and instability of Ni_2MnGa. *Phys. Solid State* **1999**, *41*, 617–623. [CrossRef]
24. Lee, Y.; Rhee, J.Y.; Harmon, B.N. Generalized susceptibility of the magnetic shape-memory alloy Ni_2MnGa. *Phys. Rev. B* **2002**, *66*, 54424. [CrossRef]
25. Bungaro, C.; Rabe, K.M.; Dal Gorso, A. First-principles study of lattice instabilities in ferromagnetic Ni_2MnGa. *Phys. Rev. B* **2003**, *68*, 134104. [CrossRef]
26. Zayak, A.T.; Entel, P.A. Critical discussion of calculated modulated structures, Fermi surface nesting and phonon softening in magnetic shape memory alloys Ni_2Mn(Ga, Ge, Al) and Co_2Mn(Ga, Ge). *J. Magn. Magn. Mater.* **2005**, *290–291*, 874–877. [CrossRef]
27. Haynes, T.D.; Watts, R.J.; Laverock, J.; Major, Z.; Alam, M.A.; Taylor, J.W.; Duffy, J.A.; Dugdale, S.B. Positron annihilation study of the Fermi surface of Ni_2MnGa. *New J. Phys.* **2012**, *14*, 035020. [CrossRef]
28. Zhao, G.L.; Harmon, B.N. Phonon anomalies in β-phase Ni_xAl_{1-x} alloys. *Phys. Rev. B* **1992**, *45*, 2818. [CrossRef]
29. Naumov, I.I.; Velikokhatnyi, O.I. Simultaneous manifestations of the 2D van Hove singularity and the Fermi surface nesting in the acoustic soft mode of β-NiAl alloys. *J. Phys. Condens. Matter* **1997**, *9*, 10339–10351. [CrossRef]
30. Huang, X.; Naumov, I.I.; Rabe, K.M. Phonon anomalies and elastic constants of cubic NiAl from first principles. *Phys. Rev. B* **2004**, *70*, 064301. [CrossRef]
31. Kakeshita, T.; Fukuda, T.; Saburi, T. Time-dependent nature and origin of displacive transformation. *Sci. Technol. Adv. Mater.* **2000**, *1*, 63–72. [CrossRef]
32. Velikokhatnyi, O.I.; Naumov, I.I.; Bashirov, V.Z. Geometric features of the Fermi surface and the premartensitic anomalies in the Hume-Rothery β-Phases. *Phys. Met. Metallogr.* **1992**, *74*, 557–564.
33. Velikokhatnyi, O.I.; Eremeev, S.V.; Naumov, I.I.; Potekaev, A.I. Long-period incommensurate superstructures in Cu–Au alloys: Relation with short-period ordering. *J. Exp. Theor. Phys.* **2000**, *90*, 479–487. [CrossRef]
34. Velikokhatnyi, O.I.; Naumov, I.I.; Eremeev, S.V.; Potekaev, A.I. Two-dimensional incommensurate superlattices in precious-metals alloys: Nature of formation. *JETP Lett.* **1999**, *69*, 589–595. [CrossRef]
35. Velikokhatnyi, O.I.; Eremeev, S.V.; Naumov, I.I.; Potekaev, A.I. Electronic structure and long period states in Ag_3Mg: Comparison with Cu–Au alloys. *J. Phys. Condens. Matter* **2000**, *12*, 8825–8830. [CrossRef]
36. Velikokhatnyi, O.I.; Eremeev, S.V.; Naumov, I.I.; Potekaev, A.I. Al_3Ti alloy: Long-period states and electronic structure. *J. Phys. Condens. Matter* **2002**, *14*, 8763–8769. [CrossRef]
37. Naumov, I.I.; Cohen, R.E.; Hemley, R.J. Graphene physics and insulator-metal transition in compressed hydrogen. *Phys. Rev. B* **2013**, *88*, 045125. [CrossRef]
38. Politano, A.; Marino, A.R.; Formoso, V.; Chiarello, G. Evidence of Kohn anomalies in quasi-freestanding graphene on Pt(111). *Carbon* **2012**, *50*, 734–736. [CrossRef]
39. Politano, A.; de Juan, F.; Chiarello, G.; Fertig, H.A. Emergence of an out-of-plane optical phonon (ZO) Kohn anomaly in quasifreestanding epitaxial graphene. *Phys. Rev. Lett.* **2015**, *115*, 075504. [CrossRef] [PubMed]
40. Struzhkin, V.V.; Timofeev, Y.A.; Hemley, R.J.; Mao, H.-K. Superconducting T_c and electron-phonon coupling in Nb to 132 GPa: Magnetic susceptibility at megabar pressures. *Phys. Rev. Lett.* **1997**, *79*, 4262–4965. [CrossRef]
41. Söderlind, P.; Moriarty, J.A. First-principles theory of Ta up to 10 Mbar pressure: Structural and mechanical properties. *Phys. Rev. B* **1998**, *57*, 10340. [CrossRef]
42. Weir, S.T.; Akella, J.; Ruddle, C.; Goodwin, T.; Hsiung, L. Static strengths of Ta and U under ultrahigh pressures. *Phys. Rev. B* **1998**, *58*, 11258. [CrossRef]

43. Cynn, H.; Yoo, C.-S. Equation of state of tantalum to 174 GPa. *Phys. Rev. B* **1999**, *59*, 8526. [CrossRef]
44. Takemura, K. Equation of state of V and Nb under truly hydrostatic conditions. In Proceedings of the International Conference on High Pressure Science and Technology (AIRAPT-17), Honolulu, HI, USA, 25–30 July 1999; Manghnani, M.H., Nellis, W.J., Nicol, M.F., Eds.; Universities Press: Hyderabad, India, 2000; pp. 443–444.
45. Ostanin, S.A.; Trubitsin, V.Y.; Savrasov, S.Y.; Alouani, M.; Dreyssé, H. Calculated Nb superconducting transition temperature under hydrostatic pressure. *Comput. Mater. Sci.* **2000**, *17*, 202–205. [CrossRef]
46. Ishizuka, M.; Iketani, M.; Endo, S. Pressure effect on superconductivity of vanadium at megabar pressures. *Phys. Rev. B* **2000**, *61*, R3823. [CrossRef]
47. Yang, L.H.; Söderlind, P.; Moriarty, J.A. Atomistic simulation of pressure-dependent screw dislocation properties in bcc tantalum. *Mater. Sci. Eng. A* **2001**, *309–310*, 102–107. [CrossRef]
48. Singh, A.K.; Takemura, K. Measurement and analysis of nonhydrostatic lattice strain component in niobium to 145 GPa under various fluid pressure-transmitting media. *J. Appl. Phys.* **2001**, *90*, 3269–3275. [CrossRef]
49. Suzuki, N.; Otani, M. Theoretical study on the lattice dynamics and electron-phonon interaction of vanadium under high pressures. *J. Phys. Condens. Matter* **2002**, *14*, 10869–10872. [CrossRef]
50. Gülseren, O.; Cohen, R.E. High-pressure thermoelasticity of body-centered-cubic tantalum. *Phys. Rev. B* **2002**, *65*, 064103. [CrossRef]
51. Louis, C.N.; Iyakutti, K. Electron phase transition and superconductivity of vanadium under high pressures. *Phys. Rev. B* **2003**, *67*, 094509. [CrossRef]
52. Nnolim, N.O.; Tyson, T.A.; Axe, L. Theory of the structural phases of group 5B–6B metals and their transport properties. *J. Appl. Phys.* **2003**, *93*, 4543–4560. [CrossRef]
53. Tse, J.S.; Li, Z.; Uehara, K.; Ma, Y. Electron phonon coupling in high-pressure Nb. *Phys. Rev. B* **2004**, *69*, 132101. [CrossRef]
54. Dewaele, A.; Loubeyre, P.; Mezouar, M. Refinement of the equation of state of tantalum. *Phys. Rev. B* **2004**, *69*, 092106. [CrossRef]
55. Dewaele, A.; Loubeyre, P. Mechanical properties of tantalum under high pressure. *Phys. Rev. B* **2005**, *72*, 134106. [CrossRef]
56. Klepeis, J.E.; Landa, A.; Söderlind, P. Electronic Topological Transitions in High-Pressure BCC Metals. In Proceedings of the 2005 APS March Meeting, Los Angeles, CA, USA, 21–25 March 2005; American Institute of Physics: College Park, MD, USA, 2005; Volume 50, p. 600.
57. Takemura, K.; Singh, A.K. High-pressure equation of state for Nb with helium-pressure medium: Powder X-ray diffraction experiments. *Phys. Rev. B* **2006**, *73*, 224119. [CrossRef]
58. Orlikowski, D.; Söderlind, P.; Moriarty, J.A. First-principles thermoelasticity of transition metals at high pressure: Tantalum prototype in the quasiharmonic limit. *Phys. Rev. B* **2006**, *74*, 054109. [CrossRef]
59. Landa, A.; Klepeis, J.; Söderlind, P.; Naumov, I.; Velikokhatnyi, O.; Vitos, L.; Ruban, A. Fermi surface nesting and pre-martensitic softening in V and Nb at high pressures. *J. Phys. Condens. Matter* **2006**, *18*, 5079–5085. [CrossRef]
60. Landa, A.; Klepeis, J.; Söderlind, P.; Naumov, I.; Velikokhatnyi, O.; Vitos, L.; Ruban, A. Ab initio calculations of elastic constants of the bcc V–Nb system at high pressures. *J. Phys. Chem. Solids* **2006**, *67*, 2056–2064. [CrossRef]
61. Suzuki, N.; Otani, M. The role of the phonon anomaly in the superconductivity of vanadium and selenium under high pressures. *J. Phys. Condens. Matter* **2007**, *19*, 125206. [CrossRef]
62. Ding, Y.; Ahuja, R.; Shu, J.; Chow, P.; Luo, W.; Mao, H.K. Structural phase transition of vanadium at 69 GPa. *Phys. Rev. Lett.* **2007**, *98*, 085502. [CrossRef] [PubMed]
63. Luo, W.; Ahuja, R.; Ding, Y.; Mao, H.K. Unusual lattice dynamics of vanadium under high pressure. *Proc. Natl. Acad. Sci. USA* **2007**, *104*, 16428–16431. [CrossRef] [PubMed]
64. Lee, B.; Rudd, R.E.; Klepeis, J.E.; Söderlind, P.; Landa, A. Theoretical confirmation of a high-pressure rhombohedral phase in vanadium metal. *Phys. Rev. B* **2007**, *75*, 180101. [CrossRef]
65. Lee, B.; Rudd, R.E.; Klepeis, J.E.; Becker, R. Elastic constants and volume changes associated with two high-pressure rhombohedral phase transformations in vanadium. *Phys. Rev. B* **2008**, *77*, 134105. [CrossRef]
66. Rudd, R.E.; Klepeis, J.E. Multiphase improved Steinberg-Guinan model for vanadium. *J. Appl. Phys.* **2008**, *104*, 093528. [CrossRef]
67. Verma, A.K.; Modak, P. Structural phase transitions in vanadium under high pressure. *Europhys. Lett.* **2008**, *81*, 37003. [CrossRef]

68. Qiu, S.L.; Marcus, P.M. Phases of vanadium under pressure investigated from first principles. *J. Phys. Condens. Matter* **2008**, *20*, 275218. [CrossRef] [PubMed]
69. Koči, L.; Ma, Y.; Oganov, A.R.; Souvatzis, P.; Ahuja, R. Elasticity of the superconducting metals V, Nb, Ta, Mo, and W at high pressure. *Phys. Rev. B* **2008**, *77*, 214101. [CrossRef]
70. Bosak, A.; Hoesch, M.; Antonangeli, D.; Farber, D.L.; Fischer, I.; Krisch, M. Lattice dynamics of vanadium: Inelastic X-ray scattering measurements. *Phys. Rev. B* **2008**, *78*, 020301. [CrossRef]
71. Landa, A.; Söderlind, P.; Ruban, A.V.; Peil, A.V.; Vitos, L. Stability in BCC transition metals: Madelung and band-energy effects due to alloying. *Phys. Rev. Lett.* **2009**, *103*, 235501. [CrossRef] [PubMed]
72. Vekilov, Y.K.; Krasil'nikov, O.M. Structural transformations in metals at high compression ratios. *Phys. Usp.* **2009**, *52*, 831–834. [CrossRef]
73. Antonangeli, D.; Farber, D.L.; Said, A.H.; Benedetti, L.R.; Aracne, C.M.; Landa, A.; Söderlind, P.; Klepeis, J.E. Shear softening of tantalum at megabar pressures. *Phys. Rev. B* **2010**, *82*, 132101. [CrossRef]
74. Bondarenko, N.G.; Vekilov, Y.K.; Isaev, E.I.; Krasil'nikov, O.M. Deformation Phase Transition in Vanadium under High Pressure. *JETP Lett.* **2010**, *91*, 611–613. [CrossRef]
75. Klepeis, J.-H.P.; Cynn, H.; Evans, W.J.; Rudd, R.E.; Yang, L.H.; Liermann, H.P.; Yang, W. Diamond anvil cell measurement of high-pressure yield strength of vanadium using in situ thickness determination. *Phys. Rev. B* **2010**, *81*, 134107. [CrossRef]
76. Landa, A.; Söderlind, P.; Velikokhatnyi, O.I.; Naumov, I.I.; Ruban, A.V.; Peil, O.E.; Vitos, L. Alloying-driven phase stability in group-VB transition metals under compression. *Phys. Rev. B* **2010**, *82*. [CrossRef]
77. Jenei, Z.; Liermann, H.P.; Cynn, H.; Klepeis, J.-H.P.; Baer, B.J.; Evans, W.J. Structural phase transition in vanadium at high pressure and high temperature: Influence of nonhydrostatic conditions. *Phys. Rev. B* **2011**, *83*, 054101. [CrossRef]
78. Krasil'nikov, O.M.; Vekilov, Y.K.; Isaev, E.I.; Bondarenko, N.G. Theory of elastic phase transitions in metals at high pressures. Application to vanadium. *J. Exp. Theor. Phys.* **2011**, *112*, 240–245. [CrossRef]
79. Liu, Z.; Shang, J. First principles calculations of electronic properties and mechanical properties of bcc molybdenum and niobium. *Rare Met.* **2011**, *30*, 354–358. [CrossRef]
80. Singh, A.K.; Liermann, H.-P. Strength and elasticity of niobium under high pressure. *J. Appl. Phys.* **2011**, *109*, 113539. [CrossRef]
81. Liu, Z.-H.; Shang, J.-X. Elastic properties of Nb-based alloys by using the density functional theory. *Chin. Phys. B* **2012**, *21*, 016202. [CrossRef]
82. Krasil'nikov, O.M.; Vekilov, Y.K.; Mosyagin, I.Y.; Isaev, E.I.; Bondarenko, N.G. Elastic phase transitions in metals at high pressures. *J. Phys. Condens. Matter* **2012**, *24*, 195402. [CrossRef] [PubMed]
83. Hu, J.; Dai, C.; Yu, Y.; Liu, Z.; Tan, Y.; Zhou, X.; Tan, H.; Cai, L.; Wu, Q. Sound velocity measurements of tantalum under shock compression in the 10–110 GPa range. *J. Appl. Phys.* **2012**, *111*, 033511. [CrossRef]
84. Guerrero, O.; Marucho, M. Elastic-Plastic transition under uniaxial stress BCC tantalum. *J. Mater. Sci. Eng. B* **2013**, *3*, 153–160.
85. Yu, Y.; Tan, Y.; Dai, C.; Li, X.; Li, Y.; Wu, Q.; Tan, H. Phase transition and strength of vanadium under shock compression up to 88 GPa. *Appl. Phys. Lett.* **2014**, *105*, 201910. [CrossRef]
86. Zhang, L.Q.; Cheng, Y.; Niu, Z.W. Elastic properties and phonon dispersion of bcc vanadium under pressure from first principles. *J. At. Mol. Sci.* **2014**, *5*, 81–94. [CrossRef]
87. Krasil'nikov, O.M.; Vekilov, Y.K.; Lugovskoy, A.V.; Mosyagin, I.Y.; Belov, M.P.; Bondarenko, N.G. Structural transformations at high pressure in the refractory metals (Ta, Mo, V). *J. Alloy. Compd.* **2014**, *586*, S242–S245.
88. Jing, Q.; Wu, Q.; Xu, J.-A.; Bi, Y.; Liu, L.; Liu, S.; Zhang, Y.; Geng, H. Anomalous softening of yield strength in tantalum at high pressures. *J. Appl. Phys.* **2015**, *117*, 055903. [CrossRef]
89. Hamlin, J.J. Superconductivity in the metallic elements at high pressures. *Phys. C* **2015**, *514*, 59–76. [CrossRef]
90. Wang, Y.X.; Wu, Q.; Xiang, R.; Chen, X.R.; Geng, H.Y. Stability of rhombohedral phases in vanadium at high-pressure and high-temperature: First-principles investigations. *Sci. Rep.* **2016**, *6*, 32419. [CrossRef] [PubMed]
91. Antonangeli, D.; Farber, D.L.; Bosak, A.; Aracne, C.M.; Ruddle, D.G.; Krisch, M. Phonon triggered rhombohedral lattice distortion in vanadium at high pressure. *Sci. Rep.* **2016**, *6*, 31887. [CrossRef] [PubMed]
92. Wang, Y.X.; Geng, H.Y.; Wu, Q.; Chen, X.R.; Sun, Y. First-principles investigation of elastic anomalies in niobium at high pressure and temperature. *J. Appl. Phys.* **2017**, *122*, 235903. [CrossRef]
93. Landau, L.D.; Lifshitz, E.M. *Statistical Physics*; Pergamon Press: Oxford, UK, 1980; Volume 1.

94. Nakagawa, Y.; Woods, A.D.B. Lattice Dynamics of Nb. *Phys. Rev. Lett.* **1963**, *11*, 271–274. [CrossRef]
95. Woods, A.D.B. Lattice dynamics of tantalum. *Phys. Rev.* **1964**, *136*, A781–A783. [CrossRef]
96. Bosak, A.; European Synchrotron Radiation Facility, Grenoble, France. Personal communication, 2010.
97. Powell, B.M.; Martel, R.; Woods, A.D.B. Lattice Dynamics of Niobium-Molybdenum Alloys. *Phys. Rev.* **1968**, *171*, 727–736. [CrossRef]
98. Powell, B.M.; Martel, R.; Woods, A.D.B. Phonon properties of niobium, molybdenum, and their alloys. *Can. J. Phys.* **1977**, *55*, 1601–1612. [CrossRef]
99. Ahuja, R.; Söderlind, P.; Trygg, J.; Melsen, J.; Wills, J.M.; Johansson, B.; Eriksson, O. Influence of pseudocore valence-band hybridization on the crystal-structure phase stabilities of transition metals under extreme compressions. *Phys. Rev. B* **1994**, *50*, 14690. [CrossRef]
100. Steinberg, D.J.; Cochran, S.G.; Guinan, M.W. A constitutive model for metals applicable at high-strain rate. *J. Appl. Phys.* **1980**, *51*, 1498–1504. [CrossRef]
101. Fridel, J. Electronic structure of primary solid solutions in metals. *Adv. Phys.* **1954**, *3*, 446–507. [CrossRef]
102. Pettifor, D.G. Theory of the crystal structures of transition metals. *J. Phys. C* **1970**, *3*, 367–377. [CrossRef]
103. Skriver, H.L. Crystal structure from one-electron theory. *Phys. Rev. B* **1985**, *31*, 1909–1923. [CrossRef]
104. Söderlind, P.; Ahuja, R.; Erikson, O.; Wills, J.M.; Johansson, B. Crystal structure and elastic-constant anomalies in the magnetic 3d transition metals. *Phys. Rev. B* **1994**, *50*, 5918. [CrossRef]
105. Clatterbuck, D.; Krenn, C.; Cohen, M.; Morris, J. Phonon instabilities and the ideal strength of aluminum. *Phys. Rev. Lett.* **2003**, *91*, 135501. [CrossRef] [PubMed]
106. Li, J.; Zhu, T.; Yip, S.; Van Vliet, K.J.; Suresh, S. Elastic criterion for dislocation nucleation. *Mater. Sci. Eng. A* **2004**, *365*, 25–30. [CrossRef]
107. Landa, A.; Söderlind, P.; Yang, L.H. Ab initio phase stability at high temperatures and pressures in the V–Cr system. *Phys. Rev. B* **2014**, *89*, 020101. [CrossRef]
108. Dai, C.; Jin, X.; Zhou, X.; Liu, J.; Hu, J. Sound velocity variations and melting of vanadium under shock compression. *J. Phys. Appl. Phys.* **2001**, *34*, 3064–3070. [CrossRef]
109. Errandonea, D.; Schwager, B.; Ditz, R.; Gessmann, C.; Boehler, R.; Ross, M. Systematics of transition-metal melting. *Phys. Rev. B* **2001**, *63*, 132104. [CrossRef]
110. Okamoto, H. N-V (Nitrogen-Vanadium). *J. Phase Equilibria* **2001**, *22*, 362–364. [CrossRef]
111. Kubel, F.; Lengauer, W.; Yvon, K.; Knorr, K.; Junod, A. Structural phase transition at 205 K in stoichiometric vanadium nitride. *Phys. Rev. B* **1988**, *38*, 12908–12912. [CrossRef]
112. Wolf, W.; Podloucky, R.; Antretter, T.; Fisher, F.D. First-principles study of elastic and thermal properties of refractory carbides and nitrides. *Philos. Mag. B* **1999**, *79*, 839–858. [CrossRef]
113. Isaev, E.I.; Simak, S.I.; Abrikosov, I.A.; Ahuja, R.; Vekilov, Y.K.; Katsnelson, M.I.; Lichtenstein, A.I.; Johansson, B. Phonon related properties of transition metals, their carbides, and nitrides: A first-principles study. *J. Appl. Phys.* **2007**, *101*, 123519. [CrossRef]
114. Ivashchenko, V.I.; Turchi, P.E.A. Phonon softening and the phase transition in VN. *Phys. Rev. B* **2008**, *78*, 224113. [CrossRef]
115. Řehák, P.; Černý, M.; Holec, D. Interface-induced electronic structure toughening of nitride superlattices. *Surf. Coat. Technol.* **2017**, *325*, 410–416. [CrossRef]
116. Mei, A.B.; Hellman, O.; Wireklint, N.; Schlepütz, C.M.; Sangiovanni, D.G.; Alling, B.; Rockett, A.; Hultman, L.; Petrov, I.; Greene, J.E. Dynamic and structural stability of cubic vanadium nitride. *Phys. Rev. B* **2015**, *91*, 054101. [CrossRef]
117. Kubel, F.; Flack, H.D.; Yvon, K. Electron densities in VN. I. High-precission X-ray diffraction determination of the valence-electron density distribution and atomic displacement parameters. *Phys. Rev. B* **1987**, *36*, 1415. [CrossRef]
118. Zheng, Q.; Mei, A.B.; Tuteja, M.; Sangiovanni, D.G.; Hultman, L.; Petrov, I.; Greene, J.E.; Cahill, D.G. Phonon and electron contributions to the thermal conductivity of VN_x epitaxial layers. *Phys. Rev. Mater.* **2017**, *1*, 065002. [CrossRef]